



Interannual Variation of Half-Hourly Extreme Precipitation in Africa: The Assessment of the Warmest Decade (2011–2020) Since the Beginning of Observations

Xolile Nciphha^{1,2} · Andries Kruger³ · Linda Sibali²

Received: 29 October 2023 / Revised: 4 January 2024 / Accepted: 14 January 2024 / Published online: 12 March 2024
© The Author(s) 2024

Abstract

Africa is experiencing widespread extreme precipitation. However, the continent remains understudied regarding extreme precipitation variation, particularly at high temporal resolution. This study assessed the changes in spatial distribution, frequency, and intensity of half-hourly violent precipitation (≥ 50 mm/h) in Africa during 2011–2020. The data were sourced from the Integrated MultisatellitE Retrievals for Global Precipitation Measurement (IMERG) program. The results reflect that the 50–60 mm/h precipitation category was the most densely spatially distributed with less-discernable interannual changes. There was a strong interannual variation in the spatial distribution of the 60–70 mm/h and ≥ 70 mm/h precipitation categories. There was a general decrease in the frequency of occurrence of violent precipitation in all regions, except in North Africa (NA). Among the study regions, NA had the broadest precipitation intensity distribution extended to high values and consequently, on average, the most intense violent precipitation, followed by Southern Africa (SA) and Southwest Indian Ocean (SWIO). The regions in the tropics, i.e., West Africa (WA), Central Africa (CA), and East Africa (EA), had a relatively narrow intense violent precipitation distribution. The results further illustrate that the strength of climate variability modes has a strong influence in the distribution, frequency, and intensity of violent precipitation over the continent particularly the ≥ 70 mm/h precipitation category. This study underscores a need for a strengthened capacity in forecasting climate variability modes impacting on Africa, augmentation of continental precipitation observation network, and improved extreme precipitation adaptation infrastructure.

Keywords Violent precipitation · Spatial distribution · Frequency · Intensity · Climate variability modes

1 Introduction

Africa is already experiencing widespread impacts from anthropogenic climate change (Trisos et al. 2022). The global and Africa's annual average temperatures were warm, reaching previous years records and setting new ones,

making the last decade (2011–2020) the warmest since the establishment of meteorological observations. In Africa, this relatively warm period was accompanied by widespread climate extremes, including flood-inducing extreme precipitation (Diasso and Njau 2015, 2016; Meque 2017; Ogwang 2018; Ogwang et al. 2019; World Meteorological Organization (WMO) 2012, 2013, 2014, 2015a, b, 2016, 2017, 2018, 2019, 2020a, b, 2021a, b). In the last 2 decades (2002–2021), floods and droughts represented 55% of natural hazard events in Africa, but floods occurring disproportionately more frequent [Centre for Research on Epidemiology of Disasters (CRED) 2022]. Floods from extreme precipitation are the most devastating natural disaster type in terms of number of affected people, as they are more frequent (Westra et al. 2014; Kimambo et al. 2019; Schumacher 2018; CRED 2022). As a result, many countries in Africa are disproportionately vulnerable to extreme precipitation, as its people livelihoods and economic sectors are negatively

✉ Xolile Nciphha
Xolile.Nciphha@weathersa.co.za

¹ South African Weather Service, Private Bag X097, Pretoria 0001, South Africa

² Department of Environmental Sciences, School of Ecological and Human Sustainability, College of Agriculture and Environmental Sciences, University of South Africa, Florida, South Africa

³ Department of Geography, Geoinformatics and Meteorology, Faculty of Natural and Agricultural Sciences, University of Pretoria, Pretoria, South Africa

impacted by it due to limited extreme climate adaptation infrastructure (Donat et al. 2013; Ford et al. 2015; Nasri et al. 2016; Zahiri et al. 2016; Fowler et al. 2021; Munyai et al. 2021; Palmer et al. 2023). The most affected regions in the last decade were West Africa (WA), Central Africa (CA), and East Africa (EA). The widespread extreme precipitation events led to floods that caused many human fatalities, injuries and displacements, infrastructure and properties damage, crop and livestock losses, and outbreak of waterborne diseases (Diasso and Njau 2015, 2016; Meque 2017; Ogwang 2018, Ogwang et al. 2019; WMO 2012, 2013, 2014, 2015a, b, 2016, 2017, 2018, 2019, 2020a, b, 2021a, b; CRED 2022; Kimutai et al. 2022).

With the warming climate, extreme daily precipitation frequency and intensity are reported to have increased in most continents since 1950 (Westra et al. 2014; Fowler et al. 2021; Gimeno et al. 2022). However, some studies suggested that the rise in frequency of extreme rainfall was much greater than the increase in intensity (Fowler et al. 2021; Gimeno et al. 2022). As the climate is still warming, extreme precipitation is expected to become even more frequent, reaching new records throughout the twenty-first century (Gimeno et al. 2022). The global mean of the twentieth and early twenty-first century rate of increase in annual maximum daily precipitation intensity was recently estimated to be 5.9–7.7%/°C of globally averaged near-surface atmospheric temperature rise (Westra et al. 2014; Schumacher 2018). The general circulation models' (GCMs) outputs also indicate that extreme precipitation intensities will increase with global warming (Westra et al. 2014). The global increase of extreme precipitation with global warming is based on the understanding of the increase in capacity of the atmosphere to hold more water vapor. This relationship is explained by the Clausius–Clapeyron (CC) equation, which determines the saturation specific humidity of the atmosphere to be dependent on temperature, increasing at a rate of 7%/°C of warming near the Earth's surface (Westra et al. 2014; Schumacher 2018; Fowler et al. 2021; Tabari 2020; Gimeno et al. 2022). However, the scaling rate of extreme precipitation with surface temperature is not one directional. Water availability also plays a vital role in the moisture–temperature relationship, where a negative scaling rate of extreme precipitation (due to dry conditions) with warming surface temperatures has been observed in some places (Fowler et al. 2021; Tabari 2020). In Africa, the inter-annual variation of extreme precipitation is modulated by the variation of various interacting complex climate variability modes, operating at regional and global scales. Several studies have provided descriptions of their mechanisms, dynamics, and impacts over various regions of the continent (e.g., Hurrell et al. 2003; Donat et al. 2013; Sylla et al. 2013; Preethi et al. 2015; Efon et al. 2016; Funk et al. 2016; Chen et al. 2019; Kuete et al. 2019; Djebbar et al. 2020; Quagraine

et al. 2020; Sazib et al. 2020; Ficchi et al. 2021; Moihamette et al. 2022; Palmer et al. 2023).

Extreme daily precipitation frequency and intensity changes have been studied in most continents (Westra et al. 2014; Fowler et al. 2021; Gimeno et al. 2022; McBride et al. 2022), including at sub-daily (primarily hourly) temporal resolution (Fowler et al. 2021). However, Africa, due to its inadequate observation networks, remains relatively understudied regarding extreme precipitation variation, particularly at high temporal resolution. Considering that short-duration extreme rainfall can cause flash floods which are often coupled with disasters (Westra et al. 2014; Kimambo et al. 2019; Fowler et al. 2021), it is imperative that all potential or possible data sources be analysed with regards to the prevalence of these events. Previous studies have assessed the increasing frequency of ENSO events in recent decades. However, the changes in the strength of El Niño (La Niña) events impact on extreme precipitation have not been considered much (Dogar et al. 2017).

This study investigated the interannual changes in spatial distribution, frequency, and intensity of half-hourly violent precipitation (≥ 50 mm/h) (Wang et al. 2021) in Africa during the warmest decade (2011–2020), using IMERG data from the Global Precipitation Measurement (GPM) mission (Huffman et al. 2018, 2019; Zhou et al. 2019). According to our knowledge, this is the first time these data have been utilised in Africa for such analysis. This period includes the occurrence of exceptionally strong El Niño and La Niña events on record (WMO 2012, 2013, 2016). Consequently, the study also examined the influence of the strength of climate variability modes on the frequency and intensity of violent precipitation over the African continent.

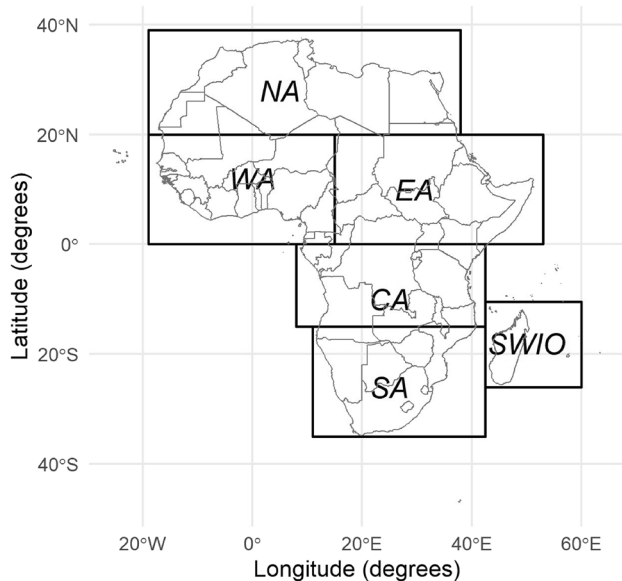
2 Material and Methods

2.1 Integrated Multisatellite Retrievals for GPM (IMERG)

This study used Final Precipitation Level 3 half-hourly data from the GPM mission. GPM is an international network of satellites of low Earth orbit carrying passive microwave sensors and geosynchronous Earth orbit with infrared sensors. The GPM program is a successor of the Tropical Rainfall Measuring Mission (TRMM) which was decommissioned in April 2015. Precipitation estimates from the GPM satellites constellation are merged by the Integrated Multi-satellite Retrievals for GPM (IMERG) algorithm produced by the U.S. GPM Science Team to produce a multi-satellite precipitation product of $0.1^\circ \times 0.1^\circ$ (roughly 10×10 km) and 30 min resolution. This study used data produced by the current version of IMERG Version 06B. The final/research version of IMERG data is adjusted to the large area-mean

Table 1 African study regions geographic demarcations

Region	Longitude range	Latitude range
NA	19° W–38° E	39° N–20° N
WA	19° W–15° E	20° N–0°
EA	15° E–53° E	20° N–0°
CA	8° E–42.5° E	0°–15° S
SA	11° E–42.5° E	15° S–35° S
SWIO	42.5° E–60° E	10.5° S–26° S

**Fig. 1** The six study regions of Africa: NA, WA, CA, EA, SA, and the SWIO

of the gauge analysis, from areas with adequate coverage of surface observations to provide regionalization and bias correction to the satellite estimates (Huffman et al. 2018, 2019; Zhou et al. 2019). The data were sourced from the NASA GES DISC website (Huffman et al. 2019). Further comparison of the IMERG data with ground-based rain gauge data was not conducted.

2.2 Study Regions

The analysis of IMERG data was conducted within the African domain, bounded by 19° W–60° E longitude and 39° N–35° S latitude. For the objective of regional analysis, Africa was divided into six regions, i.e., NA (Northern Africa), WA (Western Africa), CA (Central Africa), EA (Eastern Africa), SA (Southern Africa), and the SWIO (Southwest Indian Ocean). Table 1 and Fig. 1 show the regions and their demarcations. The boundaries of these study regions include the adjacent ocean along the coastlines according to the rectangular demarcation blocks.

2.3 Data Analysis

The 30 min resolution daily period data sets within the African domain (19° W–60° E, 39° N–35° S) were joined to make ten annual data sets from 2011 to 2020. Then, the precipitation data that were less than 50 mm/h were filtered out to produce data sets of violent precipitation (≥ 50 mm/h) (Wang et al. 2021). From these data sets, three categories of violent precipitation were prepared through data filtering, i.e., 50–60 mm/h, 60–70 mm/h, and ≥ 70 mm/h. To present an impression of the spatial distribution, annual spatial distribution maps from 2011 to 2020 were drawn using bubble plots for each event in a specific violent precipitation category. The maps were cropped to only display precipitation within the African mainland and Southwest Indian Ocean islands.

For violent precipitation frequency analysis, annual violent precipitation data for each precipitation category were subjected to regional filtering using the defined regional demarcations (geographic coordinates) to create annual data frames of the six regions. The number of occurrences of violent precipitation in each category, year, and region was counted (by determining the size of the precipitation column) from 2011 to 2020. Line graphs were plotted to display the annual variation in the occurrence of violent precipitation in each category and region. Precipitation intensity analysis was then determined from annual violent precipitation data sets covering the study period 2011–2020. Regional data frames were created through filtering using the defined regional demarcations (geographic coordinates) and the regional data were subjected to quartile analysis through creation of boxplots.

Trends of the frequencies of events in the different violent precipitation categories were determined over the 10-year analysis period. Because the temporal variation of precipitation cannot be regarded as normally distributed, especially for drier regions, as well as the relatively short time series, a non-parametric approach was applied. The Mann–Kendall rank statistic (Kendall 1975) was applied to determine whether trends were significant at the 5% level of confidence. To use this test, we need to consider only the relative values of all terms in the series x_i under analysis. The series x_i are then replaced by their ranks k_i , such that each term is assigned a number ranging from 1 to N , the total number of terms in the data series, that reflects its magnitude relative to the magnitudes of all other terms. We then compute the statistic P for the series: Compare the rank of the first term to those of all the later terms in the series. Count up the later terms whose value exceed the present term and denote this number by n_i and so on. P is then given by the sum

$$P = \sum_{i=1}^{N-1} n_i. \quad (1)$$

The statistic τ is derived from N and P by the relation

$$\tau = \frac{4P}{N(N-1)} - 1. \quad (2)$$

τ is distributed as a Gaussian normal distribution for all N larger than about 10. It can be used as the basis of a significance test by comparison with the values

$$(\tau)_t = 0 \pm t_g \sqrt{\frac{4N+10}{9N(N-1)}}, \quad (3)$$

where t_g is the desired probability point of the Gaussian normal distribution appropriate to a two-tailed test.

Consequently, the Sen's slope estimator, due to its robustness against outliers, was used to estimate the trend magnitudes (Agarwal et al. 2021; Ray et al. 2021).

3 Results and Discussion

3.1 Spatial Distribution

3.1.1 General Spatial Distribution

As can be expected, the violent precipitation is most densely spatially distributed in the tropical region, where annual precipitation is the highest, then extending southward in a northwest-to-southeast orientation to include the SWIO region (Figs. 2, 3 and 4). This extension generally follows the spatial pattern of thunderstorm cloud bands commonly known as tropical temperate troughs (TTT) (Washington and Todd 1999; Satyaban et al. 2012; Macron et al. 2014). This orientation is more distinguishable in the precipitation categories 60–70 mm/h and ≥ 70 mm/h (Figs. 3 and 4). Along the east coast of the mainland the violent precipitation extends southward to the south coast. In contrast, the occurrence of violent precipitation was less dense along the north coast of the continent. The 50–60 mm/h category was the most densely spatially distributed with less-discernable interannual changes (Fig. 2). There is a strong interannual variation in the spatial distribution of the 60–70 mm/h and ≥ 70 mm/h categories, with the ≥ 70 mm/h category annual variation most distinguishable (Figs. 3 and 4).

3.1.2 Influence of ENSO and Tropical Cyclones on Spatial Distribution.

The years 2011 and 2012 were under the influence of La Niña conditions, with the 2011 La Niña event reported to be the strongest in 60 years (WMO 2012, 2013). The

La Niña condition moderated into ENSO-neutral in 2013 (WMO 2014, 2015a). The La Niña (El Niño) conditions are associated with anomalously wet (dry) conditions over the WA, CA, SA, and SWIO regions (Joly and Voltaire 2009; Preethi et al. 2015; Randriamahefasoa and Reason 2015; Howard et al. 2019; Quagraine et al. 2020; Sazib et al. 2020; Ficchi et al. 2021; Moihamette et al. 2022); hence, the densest precipitation spatial distribution in these regions in the three years (Figs. 2, 3 and 4). In 2014, the conditions were ENSO-neutral but near El Niño (WMO 2015b), and the conditions advanced to an El Niño in 2015 which was reported to be one of the exceptionally strong events on record (WMO 2016), persisting into the early months of 2016 (WMO 2017). In EA, El Niño (La Niña) conditions result in wetter (drier) short and long rains (Palmer et al. 2023), in contrast with the regions mentioned above. Accordingly, the spatial distribution density of violent precipitation, especially the 60–70 mm/h and ≥ 70 mm/h categories, increased in 2014, 2015, and 2016 in the EA region and decreased in the WA, CA, SA, and SWIO regions (Figs. 3 and 4). In 2017 and 2018, the spatial distribution of violent precipitation was less dense at WA, CA, SA, and SWIO (Figs. 3 and 4), because of weak La Niña conditions that prevailed during that period (WMO 2018, 2019). In 2019, the distribution in WA and CA was also less dense and the precipitation extended to the EA region (Figs. 3 and 4), as a result of El Niño conditions (WMO 2020a, b). However, the distribution of violent precipitation was denser over the SWIO and the eastern part of the SA region (Figs. 3 and 4). Both regions were severely impacted by cyclones and tropical storms as the SWIO region experienced a record-breaking active cyclone season in 2019 (WMO 2020a, b). Later, the distribution was less dense in 2020 at WA, CA, SA, and SWIO because of weak La Niña conditions that developed towards the end of the year (WMO 2021a, b).

3.2 Annual Frequency

The WA, SWIO, and SA regions had the highest frequencies of occurrence of violent precipitation over the analysis period, regardless of category (Fig. 5a–c). WA experienced the highest occurrence in the categories 50–60 mm/h and 60–70 mm/h, followed by SWIO, and then the SA region (Fig. 5a and b). In the category of ≥ 70 mm/h, SWIO had the most occurrences, followed by WA, then SA (Fig. 5c). The violent precipitation occurrence in the three regions was highest in the period 2011–2013, with the peak in 2013 (Fig. 5). In the years 2011 and 2012, the climate was under the influence of strong La Niña conditions and torrential rainfalls that caused floods were reported in the three regions (WMO 2012, 2013). The year 2013 was ENSO-neutral; however, heavy falls were reported in some areas in the three regions (WMO 2014, 2015a). In 2014, the conditions

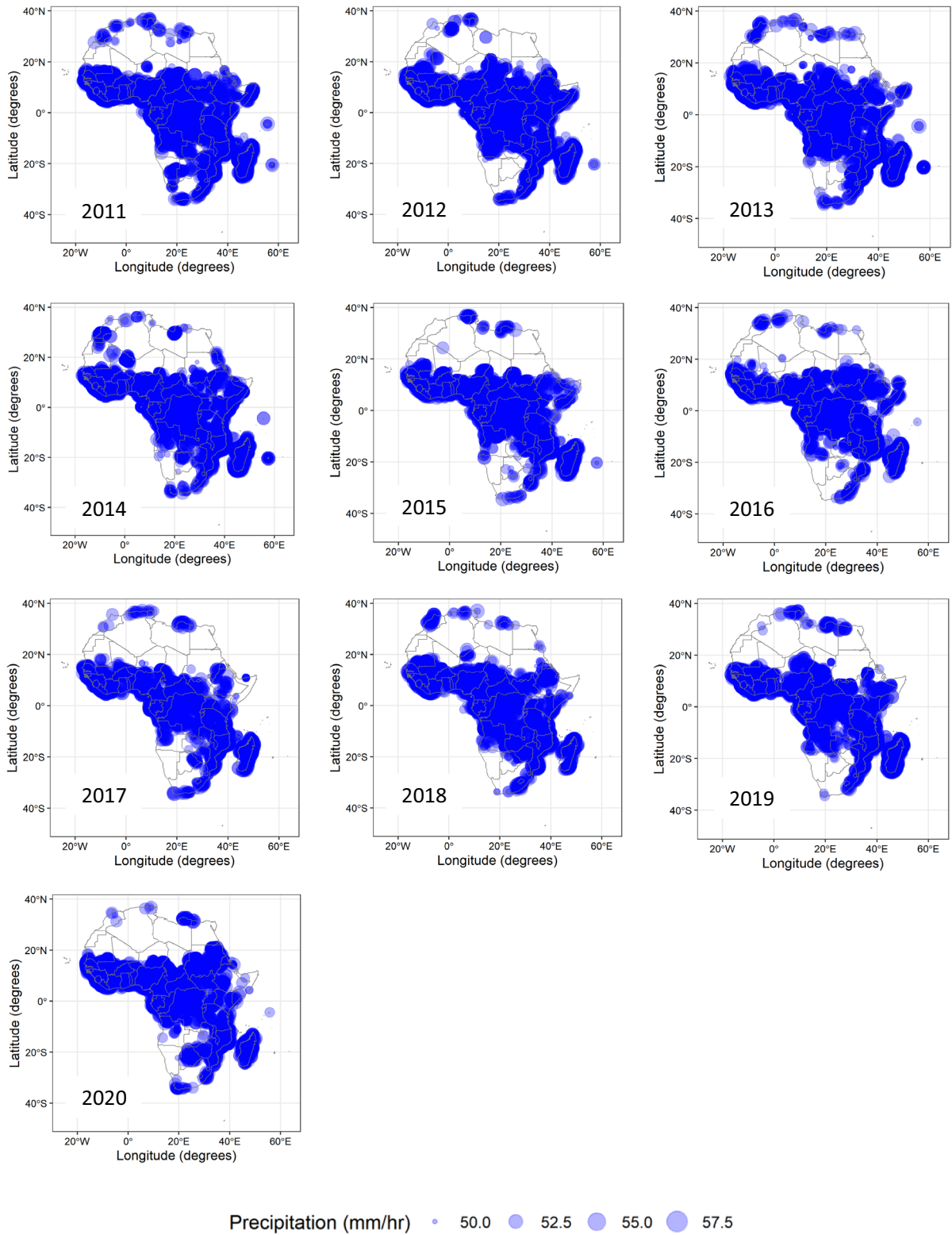


Fig. 2 The annual spatial distribution of half-hourly violent precipitation during 2011–2020 in Africa in the category 50–60 mm/h

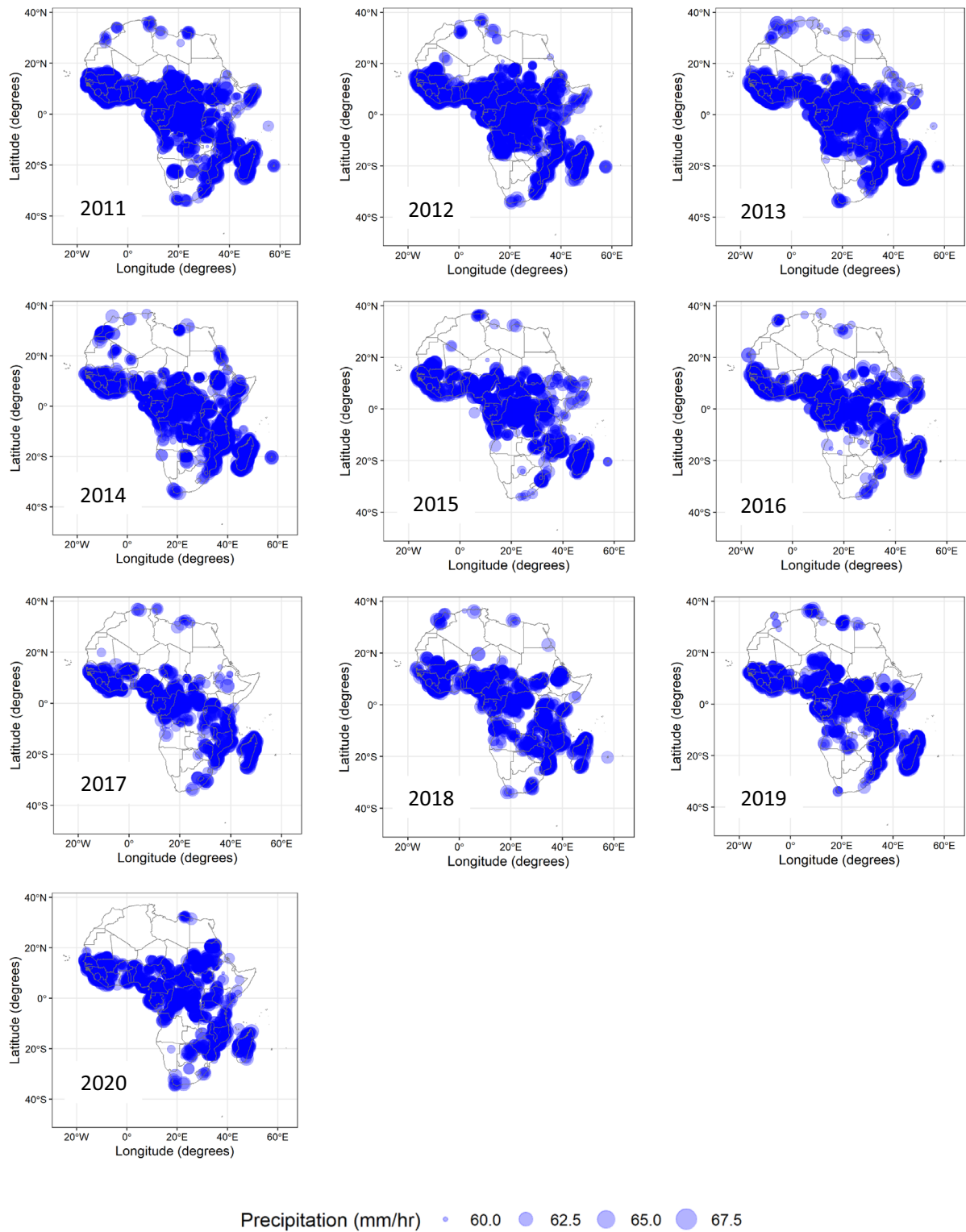


Fig. 3 The annual spatial distribution of half-hourly violent precipitation during 2011–2020 in Africa in the category 60–70 mm/h

were ENSO-neutral but near El Niño (WMO 2015b), and the conditions advanced to an exceptionally strong El Niño in 2015 (WMO 2016), which continued into the early months

of 2016 (WMO 2017). As a probable result, there were sharp continuous declines in the annual frequencies of violent precipitation in all three categories, reaching lower levels in

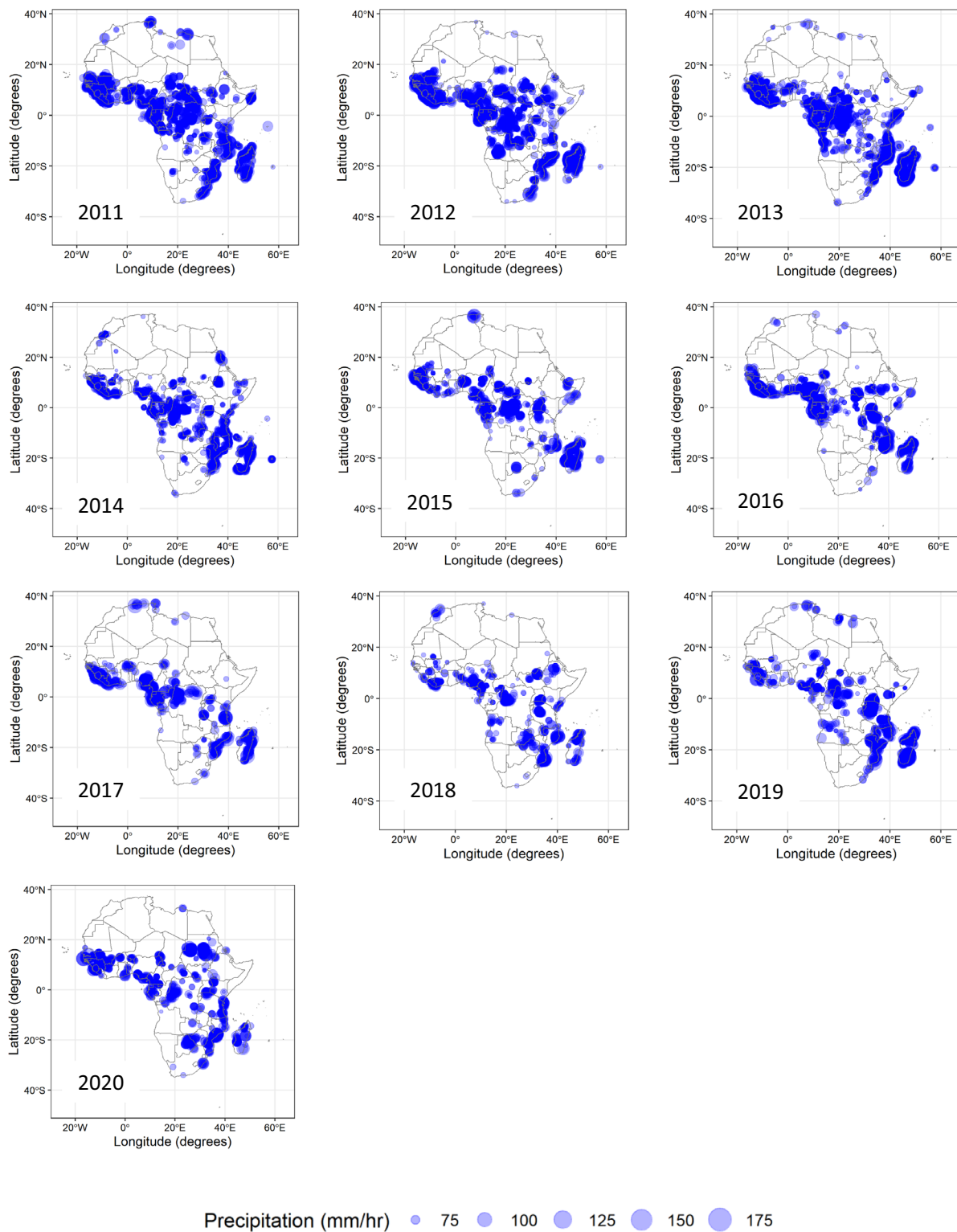


Fig. 4 The annual spatial distribution of half-hourly violent precipitation during 2011–2020 in Africa in the category ≥ 70 mm/h

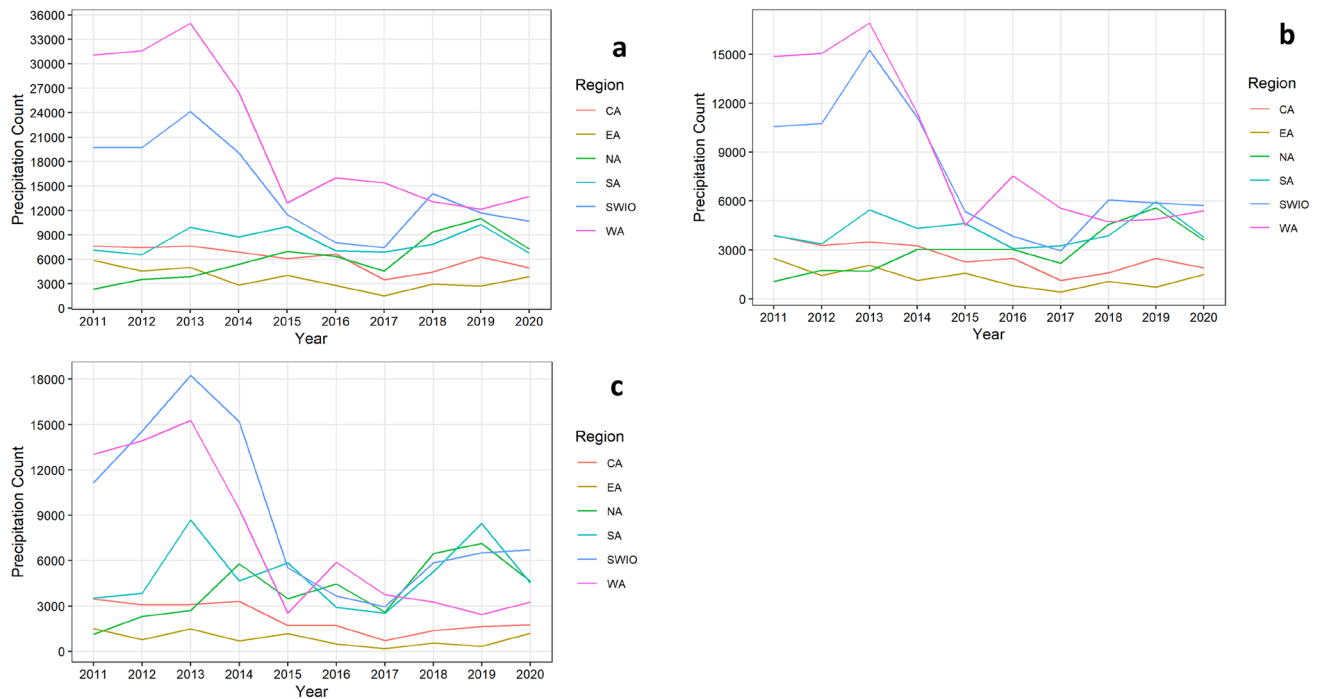


Fig. 5 Interannual variation of half-hourly violent precipitation during 2011–2020 at various regions in Africa. **a** For the category 50–60 mm/h, **b** for 60–70 mm/h, and **c** is for ≥ 70 mm/h

WA and SWIO in the years 2015 and 2017, respectively. In SA, there was no marked change in the annual frequencies of violent precipitation in the three categories from 2013 to 2015; however, there was a slight progressive drop to 2017 (Fig. 5a–c). The violent precipitation annual frequency in the three categories increased in 2016 in WA, and then, it gradually declined till 2019 and slightly increased again in 2020. The frequencies of events in the 50–60 mm/h category in WA was still clearly above the ones in SWIO and SA regions (Fig. 5a). In SWIO, the frequencies in categories 50–60 mm/h and 60–70 mm/h increased in 2018, after which they declined until 2020 (Fig. 5a and b), and the category ≥ 70 mm/h increased from 2017 to 2020 (Fig. 5c). In year 2018, the violent precipitation events in the three categories in SA increased and reached a peak in 2019 after which they declined in 2020 (Fig. 5a–c). The increase in the occurrence of violent precipitation in SA and SWIO in 2018 may have been influenced by the weak La Niña conditions that started late in 2017 and extended into 2018 (WMO 2018, 2019). The further increase in 2019, particularly in the ≥ 70 mm/h category, was probably caused by the record-breaking active tropical cyclone season in the SWIO, when several tropical cyclones and storms impacted the SWIO and SA regions (WMO 2020a, b). The decrease in the occurrence of violent precipitation in 2020 may be due to the weak El Niño conditions which were prevailing early in the year (WMO 2021a, b).

The NA, CA, and EA regions observed lesser occurrence of violent precipitation than the other regions mentioned above. Of these three regions, CA dominated with the occurrence of violent precipitation in the category 50–60 mm/h, followed by NA and then EA (Fig. 5a). In the categories 60–70 mm/h and ≥ 70 mm/h, NA recorded the highest occurrence of violent precipitation, followed by CA, then EA (Fig. 5b and c). The annual frequency of violent precipitation in the CA and EA regions generally decreased in the three categories from 2011 to 2020. Nonetheless, there were some small increases in CA and EA; in CA, they occurred in 2016, 2018 and 2019, and in EA, they occurred in 2015, 2018, and 2020. Contrarily, the annual frequency of violent precipitation in NA generally increased in the three categories from 2011 to 2020, but with 2 years of relatively low frequencies in 2017 and 2020 (Fig. 5a–c).

The 2015/2016 exceptionally strong El Niño probably influenced the increase in violent precipitation in 2015 in EA (Diasso and Njau 2016; WMO 2016, 2017). The development of the positive phase of the Indian Ocean Dipole (IOD) in 2018 and 2019 resulted in more extreme rainfall accompanied by floods and mudslides in the CA and EA regions (Ogwang et al. 2019; WMO 2020a, b; Moihamette et al. 2022; Palmer et al. 2023). The positive phase of IOD probably resulted in the increase in the occurrence of violent precipitation in CA in 2018 and 2019 (Fig. 5a–c). There was a widespread upsurge in frequency and intensity of extreme

precipitation in EA during this period, with some sites in EA which recorded historical records of extreme precipitation in 2017–2020 (Chang'a et al. 2020). The frequency change in NA is generally positive over the analysis period. The seasonal winter extreme precipitation in NA region is influenced by the negative phase of North Atlantic Oscillation (NAO) (Djebbar et al. 2020). El Niño (La Niña) conditions induce negative (positive) NAO-like patterns over the North Atlantic region which result in wet (dry) anomalies over southern Europe and NA, and the strength of the ENSO event determines the strength of the climate impact (Dogar et al. 2017). Hence, the low occurrence of violent precipitation in 2011 and 2012 (La Niña years) and peak occurrence in 2015 and 2019 (El Niño years) (Fig. 5a–c). The drop in the annual frequency of violent precipitation in the three categories in NA in 2017 and 2020 could be due to both years recording weak seasonal average negative values of NAO (Climate Prediction Center (CPC) 2023).

Following on the above and considering the climatologically short analysis period of a decade, trends in the frequencies of violent storm events are most probably determined by seasonal/annual teleconnection patterns, e.g., ENSO, than long-term climate change. Nonetheless, some significant trends could be determined at the 5% level of significance, reflecting the temporal variation of ENSO and NAO. Table 2 presents the Sen's slope for trend magnitude and Mann–Kendall results for statistical significance at the 5% level for the different precipitation magnitude categories and regions. For the 50–60 mm/h precipitation category, the only statistically significant increase is in the NA region at +892 events/year, while significant decreases occurred in the WA, EA, CA, and SWIO regions of –2361 events/year, –325 events/year, –304 events/year, and –1254 events/year, respectively. Other significant trends are: for the 60–70 mm/h category, NA: +434 events/year, WA: –1404 events/year, EA: –226 events/year, and the ≥ 70 mm/h category a similar pattern with NA: +585 events/year, WA: –1393 events/year and CA: –228 events/year.

Table 2 Sens's slope and Mann–Kendall results for the precipitation categories 50–60 mm/h, 60–70 mm/h, and ≥ 70 mm/h

CA	EA	NA	SA	SWIO	WA
50–60 mm/h					
–303.5*	–325.0*	+892.3*	+26.5	–1254.0*	–2361.3*
60–70 mm/h					
–225.5*	–170.0*	+434.3*	+1.43	–781.5	–1404.0*
≥ 70 mm/h					
–227.9*	–75.0	+584.7*	+110.4	–1150.1	–1393.0*

The numeric figures indicate the trends in annual frequency over the full analysis period (2011–2020), and the asterisk symbols (*) whether statistically significant at the 5% level of significance, according to the Mann–Kendall test

3.3 Precipitation Intensity

By the definition of violent precipitation (≥ 50 mm/h) (Wang et al. 2021), the minimum intensity was 50 mm/h throughout the study period at all regions (Fig. 6). The precipitation intensity distribution in NA gradually increased from 2011 and reached the maximum in 2014, with the 25th and 75th quartile reaching 55.8 and 83.4 mm/h, respectively. In 2015, the year was dominated by a strong positive NAO (CPC 2023), and the intensity distribution dropped to a minimum, with the 25th and 75th quartile at 53.8 and 70.4 mm/h, respectively. Then, for the rest of the following years, the 25th and 75th quartile approached 54.4 and 75 mm/h, respectively. In WA, the precipitation intensity distribution remained comparable from 2011 to 2013, with the 25th and 75th quartile values at about 54 and 69 mm/h, respectively. In 2014, it dropped and narrowed, with 25th and 75th quartile values at 53.5 and 67 mm/h, respectively. Then, in 2015, it dropped and narrowed further to a minimum, with 25th and 75th quartile values at 52.8 and 63.4 mm/h, respectively. In 2016, there was an upward shift with the 25th and 75th quartile values reaching 53.5 and 67.3 mm/h, respectively. Then, there was a drop in 2017 that was roughly maintained up until 2020, with 25th and 75th quartile values at about 53 and 64 mm/h, respectively. In CA, the precipitation intensity distribution remained relatively unchanged from 2011 to 2013, with the 25th and 75th quartile values at around 54 and 69 mm/h, respectively. In 2014, the 75th quartile shifted slightly up to 69.7 mm/h. From 2015 to 2020, the precipitation intensity distribution narrowed with the 75th quartile varying between 63 and 66.7 mm/h. The year 2017 had the smallest distribution, with the 25th and 75th quartile values at around 52.6 and 63.1 mm/h, respectively. In EA, the precipitation intensity distribution remained roughly at about 53 and 64 mm/h from 2011 to 2014 for the 25th and 75th quartile, with only a drop in the 75th quartile to about 62 mm/h in 2012. In 2015, the 75th quartile rose to the maximum of about 65.7 mm/h and dropped in 2016 to around 62 mm/h. In 2017, the precipitation intensity distribution dropped and narrowed to a minimum, with the 25th and 75th quartile values at about 52.2 and 60.6 mm/h, respectively. In 2018, it rose and widened, with the 25th and 75th quartile values at about 52.8 and 63.6 mm/h, respectively. In 2019, it dropped and narrowed, with the 25th and 75th quartile values at about 52.2 and 60.9 mm/h, respectively. Then, the distribution increased and widened in 2020, with the 25th and 75th quartile values at about 53.2 and 65.7 mm/h, respectively. The precipitation intensity distribution in SA gradually increased from 2011 and reached the maximum in 2013, with the 25th and 75th quartile reaching 55.3 and 77.9 mm/h, respectively. From 2014 to 2017, it narrowed down with 2017 distribution at minimum, with the 25th and 75th quartile values at about 53.5 and 67.2 mm/h,

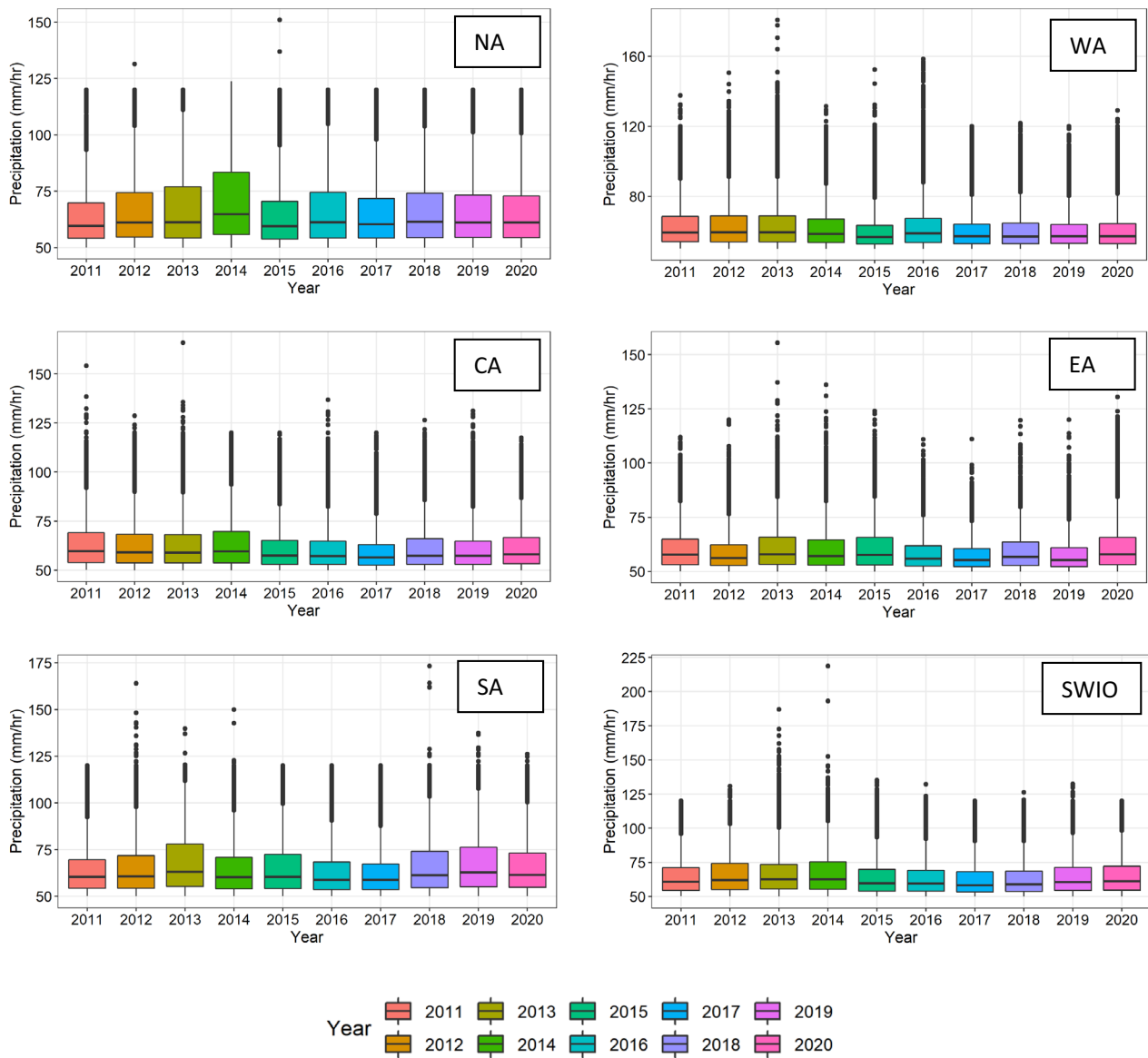


Fig. 6 Precipitation intensity distribution in NA, WA, CA, EA, SA, and SWIO regions during 2011–2020

respectively. From 2018 to 2020, it shifted up slightly and broadened, with 2019 most broad, with the 25th and 75th quartile reaching 55.2 and 76.2 mm/h, respectively. Like the case in SA, the precipitation intensity distribution in SWIO steadily increased from 2011 and reached the maximum in 2014, with the 25th and 75th quartile reaching 55.2 and 75.3 mm/h, respectively. From 2014 to 2017, it dropped and narrowed down with 2017 distribution at minimum, with the 25th and 75th quartile values at about 53.3 and 68.2 mm/h, respectively. From 2018 to 2020, it shifted up slightly and broadened, with 2020 most broad, with the 25th and 75th quartile reaching 54.6 and 72.1 mm/h, respectively. Among the study regions, NA had the broadest precipitation

intensity distribution and consequently, on average, the most intense violent precipitation, followed by SA and SWIO. The regions in the tropics, i.e., WA, CA, and EA, had a narrow intense violent precipitation distribution. Figure 6 also reflects that regions which experience anomalous wet conditions during La Niña conditions, i.e., WA, CA, SA, and SWIO, experienced a broad precipitation intensity distribution extended to high values during the 2011/2012 season of exceptionally strong La Niña conditions and a narrow distribution during the 2015/2016 season of exceptionally strong El Niño conditions. The EA region which experiences anomalous wet conditions during El Niño conditions (Palmer et al. 2023), experienced a broad precipitation

intensity distribution extended to high values during the 2015/2016 a season of exceptionally strong El Niño conditions, and a relatively narrow distribution in the 2011/2012 season with exceptionally strong La Niña conditions.

4 Summary and Conclusion

This study established a comparative analysis of the spatial distribution, frequency, and intensity of violent precipitation in different regions of Africa over the 2011–2020 decade. The results obtained reflected that violent precipitation is spatially most densely distributed in the tropical regions, extending southward in the northwest-to-southeast orientation stretching out to the adjacent SWIO region. Along the east coast of the mainland, this precipitation extends southward to the south coast. The results also indicated violent precipitation was less dense in the extreme north of the continent. The 50–60 mm/h precipitation category was found to be the most densely spatially distributed with less-discernable interannual changes, while the 60–70 mm/h and ≥ 70 mm/h categories have a strong interannual variation in spatial distribution. The study established that the strengths of ENSO events in most probability have a strong influence in the distribution of violent precipitation over the continent, particularly the most intense violent precipitation; with regions that are characteristically anomalous wet (dry) during the La Niña (El Niño) season showing a higher (lower) density during a strong La Niña (El Niño) season, conversely, regions that are characteristically anomalous wet (dry) during the El Niño (La Niña) season showing a higher (lower) density during a strong El Niño (La Niña) season. The results also demonstrated that a strong tropical cyclone season in the SWIO region contributes strongly to a dense distribution of violent precipitation in SA and SWIO.

This study indicated that the WA, SWIO and SA regions dominate with the occurrence of violent precipitation, with WA leading with events in the 50–60 mm/h and 60–70 mm/h precipitation categories, followed by SWIO and then the SA region. The SWIO has the largest occurrence of precipitation ≥ 70 mm/h, being an oceanic region with occasional strong mid-latitude and tropical cyclonic circulations, followed by WA, then SA. The NA, CA, and EA regions experience lesser occurrence of violent precipitation. The CA dominates with the precipitation category 50–60 mm/h, followed by NA and then EA. In the categories 60–70 mm/h and ≥ 70 mm/h, NA leads, followed by CA and then EA. The results also show that the magnitudes of the ENSO events have a strong influence in the frequency of violent precipitation over the continent, particularly the most intense violent precipitation; with regions that are characteristically anomalous wet (dry) during the La Niña (El Niño) season showing a higher

(lower) frequency during a strong La Niña (El Niño) season, conversely, regions that are characteristically anomalous wet (dry) during the El Niño (La Niña) season showing a higher (lower) frequency during a strong El Niño (La Niña) season. The trends in frequencies of events in the distribution categories largely reflect the influence of phases of the ENSO and NAO teleconnection patterns. Those regions which are anomalously wet during La Niña reflect negative trends due to the exceptionally strong La Niña seasons occurring at the beginning of the analysis period, while in the NA region, the positive trends reflect the NAO phase being more negative towards the end of the period.

The results of this study reflected that among the study regions, NA has the broadest precipitation intensity distribution and, on average, the most intense violent precipitation, followed by SA and SWIO. The regions in the tropics, i.e., WA, CA, and EA, have a narrow intense violent precipitation distribution. The results further illustrated that regions which experience anomalous wet (dry) conditions during La Niña conditions, i.e., WA, CA, SA, and SWIO, experience a broad precipitation intensity distribution extended to high values during exceptionally strong La Niña conditions and a narrow distribution during exceptionally strong El Niño conditions. The EA region which experiences anomalous wet conditions during El Niño conditions experiences a broad precipitation intensity distribution extended to high values during exceptionally strong El Niño conditions, and a relatively narrow distribution during exceptionally strong La Niña conditions. This extension to high values of precipitation intensity distribution increases the likelihood of occurrence of flash floods and associated disasters, particularly to low-lying terrains like coastal areas.

This study illustrates the value or usefulness of remotely sensed data like GPM (IMERG), particularly in regions like Africa that are poorly covered by in-situ ground-based observation instruments. Though the IMERG data are corrected for bias using ground-based rain gauges, some studies have indicated that the comparison of the IMERG data against rain gauge data is poor in some regions. Hence, further comparison of the IMERG data with ground-based rain gauge data is recommended in Africa in futures studies. The results of this research provide for the first time the information on the relative spatial distribution, frequency, and intensity of high temporal resolution extreme precipitation over the African continent. This information is critical for policy-makers for identifying and ranking susceptible regions to extreme short-duration precipitation (which can induce flash floods) for prioritization for observation and adaptation infrastructure establishment. This study also illustrated the influence of the strength of climate variability modes on the frequency and intensity of extreme short-duration precipitation. The study underscores a need for strengthened

capacity in forecasting of climate variability modes in Africa for extreme precipitation preparedness and augmentation of continental precipitation observation network.

Acknowledgements The authors would like to thank Goddard Earth Sciences Data and Information Services Center from National Aeronautics and Space Administration for providing the data and a special thanks to its member of staff Liu Zhong for providing guidance on how to use the data. The first author also thanks the University of South Africa for the financial support.

Author Contributions Study conception and design [Xolile Nciph]. Material preparation and data collection [Xolile Nciph] and analysis [Xolile Nciph and Andries Kruger]. The first draft of the manuscript was written by [Xolile Nciph] and all authors commented on previous versions of the manuscript. All authors read and approved the final manuscript.

Funding Open access funding provided by University of South Africa. The University of South Africa provided financial support for conference attendance to present this work and will also provide financial support for article processing charges.

Data availability The analysis data are available from the authors on request.

Declarations

Conflict of interest Andries Kruger declares he has no financial interests. Xolile Nciph has received travel support from the University of South Africa. Linda Sibali serves as a director for University of South Africa.

Ethical approval The authors declare that this work is original research; it has not been published before and that it is not under consideration for publication anywhere else; it has only been accepted as a short abstract by the Mediterranean Geoscience Union 2023 (MedGU-23) Annual meeting which was held at Istanbul (Turkey) 26–30 November. The publication of this work has been approved by all co-authors.

Open Access This article is licensed under a Creative Commons Attribution 4.0 International License, which permits use, sharing, adaptation, distribution and reproduction in any medium or format, as long as you give appropriate credit to the original author(s) and the source, provide a link to the Creative Commons licence, and indicate if changes were made. The images or other third party material in this article are included in the article's Creative Commons licence, unless indicated otherwise in a credit line to the material. If material is not included in the article's Creative Commons licence and your intended use is not permitted by statutory regulation or exceeds the permitted use, you will need to obtain permission directly from the copyright holder. To view a copy of this licence, visit <http://creativecommons.org/licenses/by/4.0/>.

References

- Agarwal S, Suchithra A, Singh SP (2021) Analysis and interpretation of rainfall trend using Mann-Kendall's and Sen's slope method. *Indian J Ecol* 48(2):453–457
- Chang'a L, Kijazi A, Mafuru K et al (2020) Understanding the evolution and socio-economic impacts of the extreme rainfall events in March–May 2017 to 2020 in East Africa. *Atmos Clim Sci* 10:553–572. <https://doi.org/10.4236/acs.2020.104029>
- Chen N, Thuat S, Hu S (2019) El Niño and the Southern Oscillation: observation. *Earth Syst Environ Sci*. <https://doi.org/10.1016/B978-0-12-409548-9.11766-X>
- Djebbar A, Goosse H, Klein F (2020) Robustness of the link between precipitation in North Africa and standard modes of atmospheric variability during the last millennium. *Climate* 8:62. <https://doi.org/10.3390/cli8050062>
- Dogar MM, Kucharski F, Azharuddin S (2017) Study of the global and regional climatic impacts of ENSO magnitude using SPEEDY AGCM. *J Earth Syst Sci* 126:30. <https://doi.org/10.1007/s12040-017-0804-4>
- Donat MG, Peterson TC, Brunet M et al (2013) Changes in extreme temperature and precipitation in the Arab region: long-term trends and variability related to ENSO and NAO. *Int J Climatol*. <https://doi.org/10.1002/joc.3707>
- Efon E, Lenouo A, Monkam D et al (2016) Cloud properties during active and break spells of the West African summer monsoon from CloudSat–CALIPSO measurements. *J Atmos Sol Terr Phys* 145:1–11. <https://doi.org/10.1016/j.jastp.2016.04.001>
- Ficchi A, Cloke H, Neves C et al (2021) Beyond El Niño: unsung climate modes drive African floods. *Weather Clim Extrem* 33:100345. <https://doi.org/10.1016/j.wace.2021.100345>
- Ford JD, Berrang-Ford L, Bunce A et al (2015) The status of climate change adaptation in Africa and Asia. *Reg Environ Change* 15(5):801–814. <https://doi.org/10.1007/s10113-014-0648-2>
- Fowler HJ, Lenderink G, Prein AF et al (2021) Anthropogenic intensification of short-duration rainfall extremes. *Nat Rev Earth Environ* 2:107–122. <https://doi.org/10.1038/s43017-020-00128-6>
- Funk C, Hoell A, Shukla S et al (2016) The East African monsoon system: seasonal climatologies and recent variations. In: de Carvalho L, Jones C (eds) *The monsoons and climate change*. Springer, Cham. https://doi.org/10.1007/978-3-319-21650-8_8
- Gimeno L, Sorí R, Vázquez M et al (2022) Extreme precipitation events. *Adv Rev WIREs Water* 9:6. <https://doi.org/10.1002/wat2.1611>
- Howard E, Washington R, Hodges K (2019) Tropical lows in Southern Africa: tracks, rainfall contributions, and the role of ENSO. *J Geophys Res* 124:11009–11032. <https://doi.org/10.1029/2019JD030803>
- Hurrell JW, Kushnir Y, Ottersen G, Visbeck M (2003) The North Atlantic Oscillation: climate significance and environmental impacts. *Geophys. Monogr. Ser.*, vol 134. AGU, Washington, DC. <https://doi.org/10.1029/134GM01>
- Joly M, Voltaire A (2009) Influence of ENSO on the West African Monsoon: temporal aspects and atmospheric processes. *J Clim* 22:3193–3210. <https://doi.org/10.1175/2008JCLI2450.1>
- Kendall MG (1975) *Rank correlation methods*. Charles Griffin, London
- Kimambo ON, Chikoore H, Gumbo R (2019) Understanding the effects of changing weather: a case of flash flood in Morogoro on January 11, 2018. *Adv Meteorol* 2019:8505903. <https://doi.org/10.1155/2019/8505903>
- Kimutai J, New M, Wolski P, Otto F (2022) Attribution of the human influence on heavy rainfall associated with flooding events during the 2012, 2016, and 2018 March–April–May seasons in Kenya. *Weather Clim Extrem* 38:100529. <https://doi.org/10.1016/j.wace.2022.100529>
- Kuete G, Pokam Mba W, Washington R (2019) African Easterly Jet South: control, maintenance mechanisms and link with Southern subtropical waves. *Clim Dyn* 54:1539–1552. <https://doi.org/10.1007/s00382-019-05072-w>

- Macron C, Pohl B, Richard Y, Bessafi M (2014) How do tropical temperate troughs form and develop over Southern Africa? *J Clim* 27:1633–1647. <https://doi.org/10.1175/JCLI-D-13-00175.1>
- McBride CM, Kruger A, Dyson L (2022) Changes in extreme daily rainfall characteristics in South Africa: 1921–2020. *Weather Clim Extrem* 38:100517. <https://doi.org/10.1016/j.wace.2022.100517>
- Moihamette F, Pokam WM, Diallo I et al (2022) Extreme Indian Ocean dipole and rainfall variability over Central Africa. *Int J Climatol* 42(10):5255–5272. <https://doi.org/10.1002/joc.75312022>
- Munyai RB, Chikoore H, Musyoki A et al (2021) Vulnerability and adaptation to flood hazards in rural settlements of Limpopo Province, South Africa. *Water* 13:3490. <https://doi.org/10.3390/w13243490>
- Nasri B, Trambly Y, Adlouni SE et al (2016) Atmospheric predictors for annual maximum precipitation in North Africa. *J Appl Meteorol Climatol* 55(4):1063–1076. <https://doi.org/10.1175/JAMC-D-14-0122.1>
- Palmer PI, Wainwright CM, Dong B et al (2023) Drivers and impacts of Eastern African rainfall variability. *Nat Rev Earth Environ* 4:254–270. <https://doi.org/10.1038/s43017-023-00397-x>
- Preethi B, Sabin T, Adedoyin J et al (2015) Impacts of the ENSO Modoki and other tropical Indo-Pacific climate-drivers on African rainfall. *Sci Rep* 5:16653. <https://doi.org/10.1038/srep16653>
- Quagrainé KA, Nkrumah F, Klein C et al (2020) West African summer monsoon precipitation variability as represented by reanalysis datasets. *Climate* 8:111. <https://doi.org/10.3390/cli8100111>
- Randriamahefasoa TSM, Resaon CJC (2015) Interannual variability of rainfall characteristics over southwestern Madagascar. *Theor Appl Climatol* 128:1–17. <https://doi.org/10.1007/s00704-015-1719-0>
- Ray S, Das SS, Mishra P, Al Khatib AMG (2021) Time series SARIMA modelling and forecasting of monthly rainfall and temperature in the south Asian countries. *Earth Syst Environ* 5:531–546
- Satyaban BR, Behera S, Ratnam JV et al (2012) An index for tropical temperate troughs over southern Africa. *Clim Dyn* 41:421–441. <https://doi.org/10.1007/s00382-012-1540-8>
- Sazib N, Mladenova IE, Bolten JD (2020) Assessing the impact of ENSO on agriculture over Africa using earth observation data. *Front Sustain Food Syst* 4:509914. <https://doi.org/10.3389/fsufs.2020.509914>
- Sylla MB, Diallo I, Pal JS (2013) West African monsoon in state-of-the-science regional climate models. In: Tarhule A (ed) *Climate variability: regional and thematic patterns*. InTech, London, pp 3–36. <https://doi.org/10.5772/55140>
- Tabari H (2020) Climate change impact on flood and extreme precipitation increases with water availability. *Sci Rep* 10:13768. <https://doi.org/10.1038/s41598-020-70816-2>
- Trisos CH, Adelekan IO, Totin E et al (2022) Africa. In: Pörtner H-O, Roberts DC, Tignor M et al (eds) *Climate change 2022: impacts, adaptation and vulnerability. Contribution of working group II to the sixth assessment report of the intergovernmental panel on climate change*. Cambridge University Press, Cambridge, pp 1285–1455. <https://doi.org/10.1017/9781009325844.011>
- Wang W, Hocke K, Mätzler C (2021) Physical retrieval of rain rate from ground-based microwave radiometry. *Remote Sens* 13:2217. <https://doi.org/10.3390/rs13112217>
- Washington R, Todd M (1999) Tropical-temperate links in southern African and Southwest Indian Ocean satellite-derived daily rainfall. *Int J Climatol* 19:1601–1616. [https://doi.org/10.1002/\(SICI\)1097-0088\(19991130\)19:14%3c1601::AID-JOC407%3e3.0.CO;2-0](https://doi.org/10.1002/(SICI)1097-0088(19991130)19:14%3c1601::AID-JOC407%3e3.0.CO;2-0)
- Westra S, Fowler HJ, Evans JP et al (2014) Future changes to the intensity and frequency of short-duration extreme rainfall. *Rev Geophys* 52:522–555. <https://doi.org/10.1002/2014RG000464>
- Zahiri EPI, Bamba AM, Famien et al (2016) Meso scale extreme rainfall events in west Africa: the cases of Niamey (Niger) and the Upper Ouémé Valley (Benin). *Weather Clim Extrem* 13:15–34. <https://doi.org/10.1016/j.wace.2016.05.001>
- Zhou Y, Nelson K, Mohr KI et al (2019) A spatial-temporal extreme precipitation database from GPM IMERG. *J Geophys Res Atmos*. <https://doi.org/10.1029/2019JD030449>
- Centre for Research on Epidemiology of Disasters (2022) The interplay of drought-flood extreme events in Africa over the last twenty years (2002–2021), CRED Crunch Newsletter, Issue No. 69. <https://www.cred.be/publications>. Accessed 16 Sept 2023
- Climate Prediction Center (2023) North Atlantic Oscillation (NAO). National Oceanic and Atmospheric Administration Centre for Weather and Climate Prediction. https://www.cpc.ncep.noaa.gov/data/teledoc/nao_ts.shtml. Accessed 16 Sept 2023
- Diasso U, Njau L (2015) State of African climate for 2014. African Center of Meteorological Applications for Development. http://acmad.net/rcc/archive_bulletin/ACMAD_bulletin_annuel_2014.pdf. Accessed 04 Oct 2023
- Diasso U, Njau L (2016) The climate in Africa 2015. Climate Change Assessment Bulletin No 2. African Center of Meteorological Applications for Development. http://acmad.net/rcc/archive_bulletin/ACMAD_bulletin_annuel_2015.pdf. Accessed 04 Oct 2023
- Huffman G J, Bolvin DT, Braithwaite D et al (2018) NASA Global Precipitation Measurement Integrated Multisatellite Retrievals for GPM (IMERG), NASA Algorithm theoretical basis document (ATBD) version 5.2. https://pmm.nasa.gov/sites/default/files/document_files/IMERG_ATBD_V5.2.pdf. Accessed 16 Sept 2023
- Huffman GJ, Stocker EF, Bolvin DT et al (2019) GPM IMERG final precipitation L3 half hourly 0.1 degree x 0.1 degree V06, Greenbelt, MD, Goddard Earth Sciences Data and Information Services Center (GES DISC). <https://doi.org/10.5067/GPM/IMERG/3B-HH/06>. Accessed 16 Sept 2023
- Meque A (2017) The climate in Africa 2016. Climate Change Assessment Bulletin N° 5. African Center of Meteorological Applications for Development. http://acmad.net/rcc/archive_bulletin/ACMAD_bulletin_annuel_2016.pdf. Accessed on 04 Oct 2023
- Ogwang BA (2018) The state of climate in Africa 2017. Climate service for increased resilience in the sahel project. Report N° 5. African Center of Meteorological Applications for Development. <https://www.acmad.net/new/sites/default/files/The-State-of-Climate-in-Africa-2017-Report-March-2018-ACMAD.pdf>. Accessed 04 Oct 2023
- Ogwang BA, Kabengwela H, Dione C, Kamga FA (2019) The state of climate of Africa in 2018. African Center of Meteorological Applications for Development. http://www.acmad.net/new/sites/default/files/The-State-of-Climate-in-Africa-2018-Report-March-2018-March2019_Final.pdf. Accessed 04 Oct 2023
- Schumacher RS (2018) Heavy rainfall and flash flooding. Oxford research encyclopedia of natural hazard science. <https://doi.org/10.1093/acrefore/9780199389407.013.132>. https://training.weather.gov/wdt/courses/ffawoc/IC1/mcs/presentation_content/external_files/Schumacher-Oxford.pdf. Accessed 16 Sept 2023.
- World Meteorological Organization (2012) WMO Statement on the status of the global climate in 2011. WMO-No. 1085. <https://digitallibrary.un.org/record/3894582?ln=en>. Accessed 19 Dec 2023
- World Meteorological Organization (2013) WMO Statement on the status of the global climate in 2012. WMO-No. 1108. <https://library.wmo.int/records/item/55986-wmo-statement-on-the-status-of-the-global-climate-in-2012>. Accessed 16 Sept 2023
- World Meteorological Organization (2014) WMO Statement on the status of the global climate in 2013. WMO-No. 1130. <https://library.wmo.int/records/item/56020-wmo-statement-on-the-status-of-the-global-climate-in-2013>. Accessed 16 Sept 2023
- World Meteorological Organization (2015a) WMO the climate in Africa: 2013. WMO-No. 1147. <https://library.wmo.int/records/item/53417-the-climate-in-africa-2013>. Accessed 16 Sept 2023

- World Meteorological Organization (2015b) WMO Statement on the status of the global climate in 2014. WMO-No. 1152. <https://library.wmo.int/records/item/56040-wmo-statement-on-the-status-of-the-global-climate-in-2014>. Accessed 16 Sept 2023
- World Meteorological Organization (2016) WMO statement on the status of the global climate in 2015. WMO-No. 1167. <https://www.unep.org/resources/report/wmo-statement-status-global-climate-2015>. Accessed 16 Sept 2023
- World Meteorological Organization (2017) WMO statement on the status of the global climate in 2016. WMO-No. 1189. <https://library.wmo.int/records/item/56097-wmo-statement-on-the-state-of-the-global-climate-in-2016>. Accessed 16 Sept 2023
- World Meteorological Organization (2018) WMO statement on the status of the global climate in 2017. WMO-No. 1212. <https://library.wmo.int/records/item/56119-wmo-statement-on-the-state-of-the-global-climate-in-2017>. Accessed 16 Sept 2023.
- World Meteorological Organization (2019) WMO statement on the status of the global climate in 2018. WMO-No. 1233. <https://library.wmo.int/records/item/56141-wmo-statement-on-the-state-of-the-global-climate-in-2018>. Accessed 16 Sept 2023
- World Meteorological Organization (2020a) State of the climate in Africa 2019. WMO-No. 1253. <https://library.wmo.int/records/item/57196-state-of-the-climate-in-africa-2019>. Accessed 16 Sept 2023
- World Meteorological Organization (2020b) WMO statement on the status of the global climate in 2019. WMO-No. 1248. <https://library.wmo.int/records/item/56228-wmo-statement-on-the-state-of-the-global-climate-in-2019>. Accessed 16 Sept 2023
- World Meteorological Organization (2021a) WMO statement on the status of the global climate in 2020. WMO-No. 1264. <https://library.wmo.int/records/item/56247-state-of-the-global-climate-2020>. Accessed 16 Sept 2023
- World Meteorological Organization (2021b) WMO The climate in Africa: 2020. WMO-No. 1275. <https://library.wmo.int/records/item/57682-state-of-the-climate-in-africa-2020>. Accessed 16 Sept 2023
- World Meteorological Organization (2011) WMO statement on the status of the global climate 2011. WMO-No. 1085. <https://library.wmo.int/records/item/56761-wmo-statement-on-the-status-of-the-global-climate-in-2011>. Accessed 16 Sept 2023